Phase Transitions in Thin Films of a Diblock Copolymer Composed of a Linear Polymer Block and a Brush Polymer Block with Mesogenic Oligothiophenyl Bristles

Jinhwan Yoon,[†] Sangwoo Jin,[†] Byungcheol Ahn,[†] Yecheol Rho,[†] Tomoyasu Hirai,[‡] Rina Maeda,[‡] Teruaki Hayakawa,*[,‡] Jehan Kim,[†] Kwang-Woo Kim,[†] and Moonhor Ree*[,†]

Department of Chemistry, National Research Laboratory for Polymer Synthesis & Physics, Pohang Accelerator Laboratory, Center for Integrated Molecular Systems, and BK School of Molecular Science, Pohang University of Science and Technology, Pohang 790-784, Republic of Korea, and Department of Organic & Polymeric Materials, Graduate School of Science and Engineering, Tokyo Institute of Technology, 2-12-1-S8-26, O-okayama, Meguro-ku, Tokyo 152-8552, Japan

Received July 29, 2008; Revised Manuscript Received September 11, 2008

ABSTRACT: In this study, we quantitatively investigated the temperature-dependent phase transition behaviors in thin films of an interesting semirod−coil diblock copolymer, poly(styrene)-*b*-poly(oligothiophene side chain modified isoprene) (PS-*b*-POTI), and the resulting morphological structures using synchrotron grazing incidence X-ray scattering combined with differential scanning calorimetry. These analyses provided detailed information about the morphologies of the phase-separated domains and the molecular structures formed in each domain. At room temperature, the diblock copolymer molecules in thin films were found to form an alternately stacked structure comprised of amorphous PS and smectic-A POTI microdomains whose stacking direction is parallel to the film plane. On heating, the films underwent a phase transformation to a hexagonal cylinder structure with cylindrical POTI domains in the PS matrix oriented normal to the film plane. This phase conversion is induced by the transformation of the POTI domains from a smectic-A phase to an isotropic phase, where the smectic-A phase is composed of a laterally ordered structure of interdigitated bristles in the POTI blocks. On the basis of these structural analysis results, we propose models for the molecular structures of the diblock polymer thin films at various temperatures.

Introduction

Block copolymer thin films present a wide range of microphase-separated morphologies depending on the volume fractions of the components, thus opening fascinating possibilities for the preparation of materials with tunable nanostructure.[1,2] In particular, much research effort has focused on the production of novel block copolymers bearing π-conjugated moieties, because of their potential applications in various fields such as optics and electronics.[3−5] These block copolymers have the advantage that they combine the properties of π-conjugated materials and block copolymers, thereby providing not only novel functionalities but also the possibility of nanostructure formation. Thus, the synthesis and characterization of π-conjugated block copolymers have been extensively studied.[3−5] Among these materials, oligo and polythiophene containing block copolymers are particularly interesting because the thiophene moiety is a typical π-conjugated group with properties such as electrical conductivity, optical storage, and photoluminescence.[4,5] Furthermore, the thiophene moiety acts as a mesogenic group in liquid crystal domains, and thus influences microphase separation due to regular ordering of the liquid crystal.

Recently, Hayakawa and co-workers[5] reported an interesting semirod−coil diblock copolymer system, poly(styrene)-*b*-poly(oligothiophene side chain modified isoprene) (PS-*b*-POTI), which is composed of a styrene block and an isoprene block with oligothiophene-modified side chains (Figure 1). This diblock polymer, when coated as a thin film on a glass slide, exhibits extremely ordered hierarchical structures from the molecular to the micrometer scale on the surface under a moist air flow. Single layers of hexagonally packed micropores were developed with a narrow size distribution (mean diameter 1.5 μm) and walls as thin as 100 nm. In the cross-section of the film, lamellar layers of polystyrene and polyisoprene blocks perpendicular to the substrate were found with a liquid-crystalline smectic mesophase of the π-stacked oligothiophene blocks. It is very important to explore and clarify the phase behavior of PS-*b*-POTI in order to understand the physical properties that it exhibits in various applications. However, structural investigations of this material have been limited to

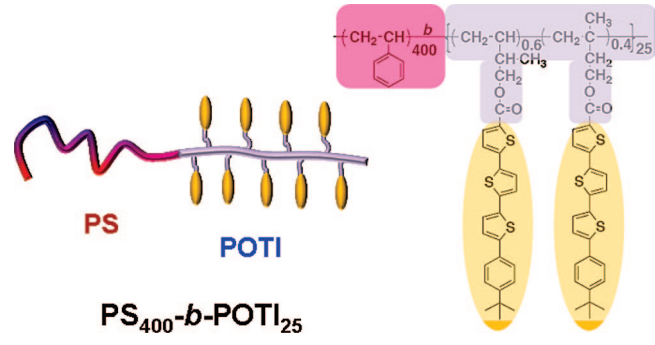

Figure 1. Chemical structure of the semi rod−coil diblock copolymer PS-*b*-POTI, consisting of polystyrene (PS) and polyisoprene with oligothiophene modified side chains (POTI).

* To whom correspondence should be addressed. E-mail: ree@postech.edu (M.R.); hayakawa@op.titech.ac.jp (T.H.). Telephone: +82-54-279-2120(M.R.); +81-3-5734-2429 (T.H.). Fax: +82-54-279-3399 (M.R.); +81-3-5734-2875 (T.H.).

[†] Department of Chemistry, National Research Laboratory for Polymer Synthesis & Physics, Pohang Accelerator Laboratory, Center for Integrated Molecular Systems, and BK School of Molecular Science, Pohang University of Science and Technology.

[‡] Department of Organic & Polymeric Materials, Graduate School of Science and Engineering, Tokyo Institute of Technology.

10.1021/ma801727r CCC: $40.75
Published on Web 10/23/2008

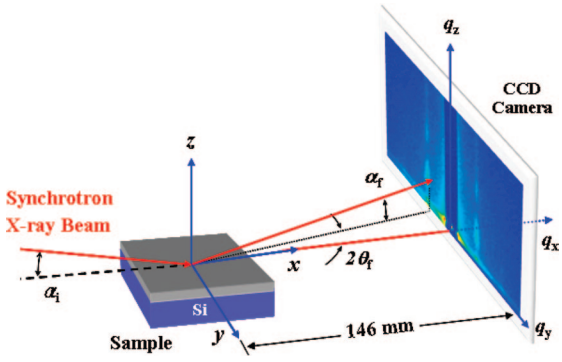

Figure 2. GIXS geometry: α_i is the incident angle at which the X-ray beam impinges on the film surface; α_f and $2\theta_f$ are the exit angles of the X-ray beam with respect to the film surface and to the plane of incidence, respectively; and q_x, q_y, and q_z are the components of the scattering vector **q**.

microscopic analysis and qualitative one-dimensional wide-angle X-ray diffraction analysis.

Here, we report the structure and orientation details of PS-*b*-POTI thin films coated on silicon substrates, which were characterized using a combination of synchrotron grazing incidence X-ray scattering (GIXS) and differential scanning calorimetry (DSC). In addition, we report the temperature-induced order-order and order−disorder structural transitions of the phase-separated domains in the diblock copolymer thin films. In particular, the liquid crystalline characteristics of the oligothiophene moiety were found to be directly related to the structures of the PS-*b*-POTI diblock copolymer thin films.

Experimental Section

Materials. The semirod−coil diblock copolymer of polystyrene (PS) and polyisoprene with oligothiophene-modified side chains (POTI), namely PS_{400}-*b*-$POTI_{25}$ was prepared by esterifying a poly(styrene-*b*-substituted isoprene) block copolymer with an oligothiophene derivative.[5] The PS-*b*-POTI product was determined to have a number average molecular weight $\bar{M}_n$ of 55 600 and a polydispersity index (PDI) of 1.08 by using a gel permeation chromatography calibrated with polystyrene standards. The dried PS-*b*-POTI product was dissolved in toluene and filtered using a disposable syringe equipped with a poly(tetrafluoroethylene(filter of pore size 0.2 μm, producing a solution of 1 wt %. This filtered solution was spin-coated onto precleaned silicon substrates and dried at 50 °C, followed by annealing at 175 °C for 1 day under vacuum. The obtained diblock copolymer films were measured to have a thickness of 25−30 nm, using a spectroscopic ellipsometer (model M2000, J. A. Woollam, Lincoln, NE) and an α-stepper (model Tektak3, Veeco, Santa Clara, CA). In addition, the two homopolymers (PS and POTI) were synthesized. The obtained PS homopolymer was determined to have 39 500 $\bar{M}_n$ and 1.07 PDI while the POTI polymer was found to have 15 800 $\bar{M}_n$ and 1.12 PDI.

Measurements. GIXS measurements were carried out at the SAXS beamlines (4C1 and 4C2)[6] at the Pohang Accelerator Laboratory.[7] The samples were measured at a sample-to-detector distance (SDD) of 2214 mm and 146 mm for small angle and wide angle region, respectively. The GIXS measurements were conducted on the film samples during heating and subsequent cooling over the temperature range 30 to 300 °C. Here the heating and subsequent cooling runs were carried out with a rate of 2.0 °C/min in vacuum. Scattering data were typically collected for 30 s using an X-ray radiation source of $\lambda = 0.154$ nm with a two-dimensional (2D) charge-coupled detector (CCD: Roper Scientific, Trenton, NJ), as shown in Figure 2. The incidence angle α_i of the X-ray beam was set at 0.18°, which is between the critical angles of the films and the silicon substrate ($\alpha_{c,f}$ and $\alpha_{c,s}$). Scattering angles were corrected according to the positions of the X-ray beams reflected from the silicon substrate interface with changing incidence angle α_i, and

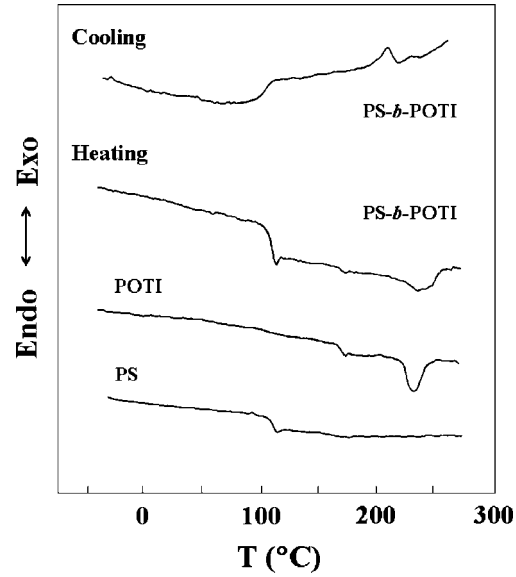

Figure 3. DSC thermograms of PS-*b*-POTI and its homopolymers. The measurements were carried out with a rate of 10.0 °C/min under a nitrogen atmosphere.

with respect to a precalibrated silver behenate (TCI, Japan) powder. Aluminum foil pieces were employed as a semitransparent beam stop, because the intensity of the specular reflection from the substrate is much stronger than the intensity of GIXS near the critical angle.

Atomic force microscopy (AFM) measurements were performed to observe topography images of the PS-*b*-POTI thin films. The spin-coated PS-*b*-POTI films were imaged using a scanning probe microscope (model Multimode Nanoscope IIIa, Veeco, Santa Clara, CA) in tapping mode, which was equipped with a JV-scanner; noncoated silicon etched probes (model LTESP, Veeco) were used in the measurements. DSC measurements were carried out at a rate of 10.0 °C/min under a nitrogen atmosphere by using a calorimeter (model DSC6200, Seiko Instruments, Japan). Nitrogen was purged at a flow rate of 50 mL/min.

Results and Discussion

The thermal behaviors of PS-*b*-POTI were investigated using DSC. Figure 3 shows typical DSC thermograms of PS-*b*-POTI, which were measured during heating followed by cooling at a rate of 10.0 °C/min. During the heating run, PS-*b*-POTI underwent three phase transitions. In comparison, on heating run PS homopolymer revealed only one transition while POTI homopolymer exhibited two transitions (Figure 3). On the DSC thermograms, the glass transition temperatures T_g of PS and POTI homopolymers were 103 and 166 °C, respectively, and the phase transition of POTI homopolymer from the smectic-A mesophase to the isotropic phase was observed at 235 °C.[5] Taking these data into account, the first two baseline shifts at 104 and 168 °C in the DSC trace of the block copolymer correspond to the glass transitions of the PS and POTI blocks respectively and the third transition at 238 °C is attributed to the transition of the smectic-A phase to the isotropic liquid phase.

During the subsequent cooling run, the diblock polymer sample was also found to exhibit three phase transitions (Figure 3). The exothermic peak in the range 210−190 °C is due to the transition from the isotropic liquid to the smectic-A phase of the POTI block, and the baseline shifts observed at 165 and 99 °C correspond to the glass transitions of the POTI and PS blocks, respectively. These DSC results confirm that the liquid-crystal transition of the POTI blocks is thermally reversible.

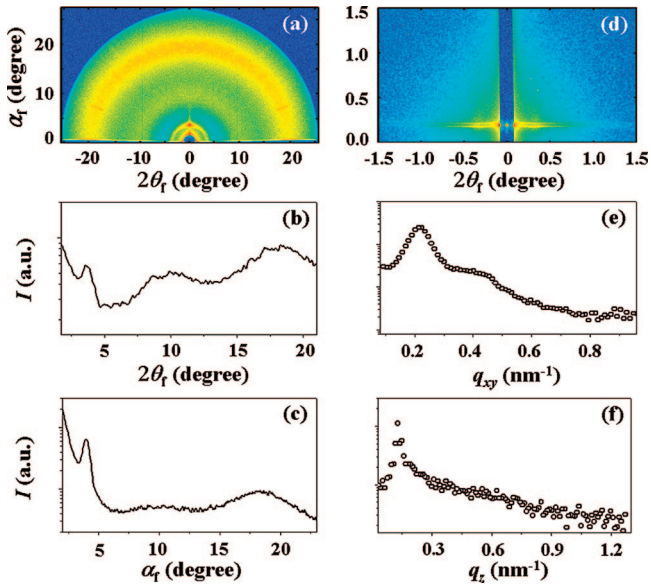

Figure 4. (a) 2D GIWAXD pattern measured at $\alpha_i = 0.18°$ for a PS-*b*-POTI thin film deposited on a silicon substrate measured at 25 °C. (b) In-plane scattering profile extracted from the GIWAXD patterns in (a) along the $2\theta_f$ direction at $\alpha_f = 0.18°$. (c) Out-of-plane scattering profile extracted from the GIWAXD pattern in (a) along the α_f direction at $2\theta_f = 0.0°$. (d) 2D GISAXS pattern measured at $\alpha_i = 0.18°$ for an PS-*b*-POTI thin film deposited on a silicon substrate measured at 25 °C. (e) In-plane scattering profile extracted from the GISAXS pattern in (d) along the $2\theta_f$ direction at $\alpha_f = 0.18°$. (f) out-of-plane scattering profile extracted from the GISAXS pattern in (d) along the α_f direction at $2\theta_f = 0.11°$.

GIXS measurements were carried out on the diblock copolymer films because GIXS is a versatile tool for obtaining structural information on the nanostructure in thin films.[8−11] To observe both the phase-separated domain structure and molecular structure in each domain, grazing incidence wide-angle scattering (GIWAXS) and grazing incidence small-angle scattering (GISAXS) measurements were performed on PS-*b*-POTI thin films.

Figure 4a shows the 2D GIWAXD pattern obtained from a diblock copolymer film at 25 °C. Parts b and c of Figure 4 show the in-plane and out-of-plane scattering profiles, which were extracted along the $2\theta_f$ direction at $\alpha_f = 0.18°$ and along the α_f direction at $2\theta_f = 0°$, respectively, from the diffraction pattern in Figure 4a. Strong scattering is clearly observed along the α_f direction at $2\theta_f = 0$ (Figure 4a), with a maximum intensity at around $\alpha_f = 3.64°$. This scattering spot indicates the presence of layered structures stacked normal to the film plane, in this case a smectic-A phase. Here, it is noted that this scattering spot also has a circular scattering ring, which may be a result of variations in the orientation of the smectic layers arising from undulation of the smectic layer surface.[10] From the location of the reflection spots, $\alpha_f = 3.64°$, the smectic layer spacing was determined to be 2.42 nm. The molecular dimension of the POTI block was estimated using a molecular simulation with the Cerius^2 software package (Accelrys, San Diego, CA). As can be seen in Figure 5a, the lengths of the oligothiophene bristle unit and the remainder of the cross section of the POTI block are 1.64 and 0.82 nm, respectively. Thus, we calculated the length of the fully extended bristle in the POTI block to be 2.05 nm. The layer spacing of 2.42 nm obtained from the GIWAXD measurement is larger than the length of the fully extended bristles (2.05 nm) in the POTI block, but much less than twice the bristle length (4.11 nm). The broad, weak peak centered at $2\theta_f = 18.30°$ corresponds to a *d*-spacing of 0.484 nm, which is equal to the interdistance between the ordered bristles of the POTI block. These results indicate that the bristles

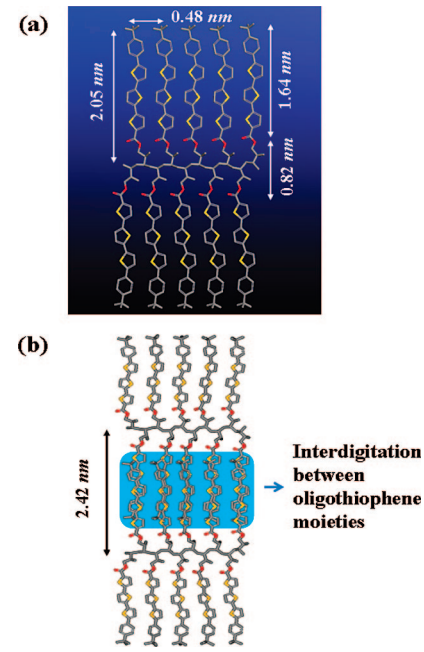

Figure 5. (a) Molecular model of the POTI block and its dimension in the fully extended conformation. The atoms are colored as follows; C, gray; O, red; S, yellow. (b) Molecular packing model of a layer structure formed in the POTI domains of a PS-*b*-POTI thin film. In this model, the oligothiophene groups in the POTI side chains are fully interdigitated.

of the POTI blocks in one smectic layer are interdigitated with those of the adjacent smectic layer in the stack. Considering the molecular dimension of the bristles in the POTI block, we conclude that the oligothiophene units in the POTI blocks are fully interdigitated (Figure 5b). In this model, the interchain distance between the polyisoprene backbone in the layer stacks is 2.46 nm, which is in good agreement with the layer spacing of 2.42 nm obtained from the GIWAXD measurement. Since oligothiophene is known to tend to aggregate through $\pi-\pi$ stacking interactions,[12] it is possible to make a stable conformation with interdigitation between the oligothiophene units in the POTI blocks.

As can be seen in Figure 4, parts b and c, two additional broad isotropic scattering peaks appear at 9.51° and 18.5°, which correspond to *d*-spacings of 0.928 and 0.484 nm, respectively. These peaks are due to the amorphous structure of the PS block at 25 °C.

These results indicate that the POTI blocks in the thin films form phase-separated domains with a well-ordered layer structure. The observed layer structure of POTI domains is assigned as the smectic-A phase. These GIWAXD analysis results confirm that, at 25 °C, the diblock copolymer film consists of amorphous PS domains and smectic-A POTI domains.

Figure 4d shows the 2D GISAXS pattern for a diblock copolymer film at 25 °C. In this figure, some weak scattering peaks are observed along the $2\theta_f$ direction, and brightly striped patterns appear along the $2\theta_f$ direction at exit angles (α_f) between the critical angles of the film and silicon substrate. These striped patterns are intense scatterings formed due to a combination of a standing wave phenomenon and total reflection at the interface between the film and the substrate, as is often observed in specular X-ray reflectivity patterns.[13] We also found that some peaks overlap with the striped patterns along the $2\theta_f$ direction, indicating the presence of periodic structures in the plane of the PS-*b*-POTI thin film.

Taking this quantitative structural information into account, we extracted the in-plane and out-of-plane scattering profiles

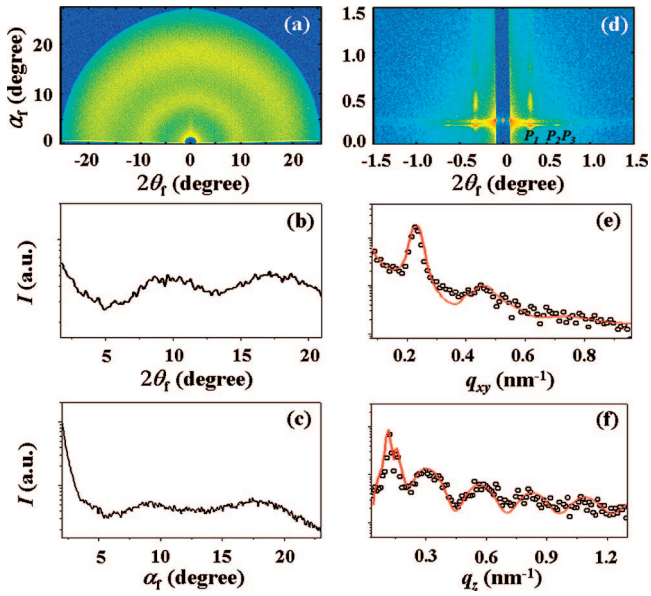

Figure 6. (a) 2D GIWAXD pattern measured at $\alpha_i = 0.18°$ for an PS-*b*-POTI thin film deposited on a silicon substrate at 245 °C. (b) In-plane scattering profile extracted from the GIWAXD pattern in (a) along the $2\theta_f$ direction at $\alpha_f = 0.18°$. (c) Out-of-plane scattering profile extracted from the GIWAXD pattern in (a) along the α_f direction at $2\theta_f = 0.0°$. (d) 2D GISAXS pattern measured at $\alpha_i = 0.18°$ for an PS-*b*-POTI thin film deposited on a silicon substrate measured at 245 °C. (e) In-plane scattering profile extracted from the GISAXS pattern in (d) along the $2\theta_f$ direction at $\alpha_f = 0.18°$. (f) Out-of-plane scattering profile extracted from the GISAXS pattern in (d) along the α_f direction at $2\theta_f = 0.31°$. The symbols are the measured data, and the solid lines were obtained by fitting the data with the GISAXS formula.

in the GISAXS pattern measured at 25 °C in Figure 4d along the $2\theta_f$ direction at $\alpha_f = 0.18°$, and along the α_f direction at $2\theta_f = 0.11°$, respectively; these profiles are shown in Figure 4, parts e and f. Whereas the out-of-plane profile is very weak and featureless, similar to the 2D GISAXS pattern, the in-plane scattering profile contains scattering peaks at 0.218 nm^{-1} and 0.440 nm^{-1} with relative scattering vector lengths from specular reflection positions of **1** and **2**. These results indicate that the lamellar layers consisting of PS and POTI blocks are stacked parallel to the film plane. The scattering peak at 0.218 nm^{-1} corresponds to a long period of the lamellar stack of 28.8 nm. However, the broad first- and second-order peaks without higher order reflections indicate that the lamellae are poorly packed together.

Collectively the GIWAXD and GISAXS results indicate that lamellae consisting of amorphous PS and smectic-A POTI microdomains are alternately stacked perpendicular to the film plane at 25 °C.

To elucidate the temperature dependence of the nanostructure of the PS-*b*-POTI thin film, GIXS measurements were carried out during a heating run and subsequent cooling run. During the heating run, the scattering pattern was found to retain its shape and intensity from 25 °C up to 245 °C. Above 245 °C, the isotropic transition temperature of the smectic-A phase, the 2D GIWAXD and GISAXS patterns underwent drastic changes.

Figure 6a shows the 2D GIWAXD pattern of a diblock copolymer film recorded at 245 °C. At this temperature, the GIWAXS pattern is very weak and featureless except for two broad isotropic scattering peaks. These broad and weak diffraction rings are attributed to both the PS and POTI blocks having amorphous structures at 245 °C, as discussed in relation to the DSC thermogram. Figures 6b and 6c show the in-plane and out-of-plane scattering profiles, which were extracted along the $2\theta_f$ direction at $2\theta_f = 0.18°$ and along the α_f direction at $2\theta_f = 0°$, respectively, from the diffraction pattern in Figure 6a. When the temperature of the film reaches 245 °C, the diffraction peak arising from the mesophase of the POTI domains has completely disappeared, and only two amorphous halo rings are present. The first peak at 9.5° (*d*-spacing = 0.93 nm) and the second peak at 18.7° (*d*-spacing = 0.48 nm) are assigned to the amorphous halo of the PS block, and the overlap of the amorphous haloes of PS and POTI blocks, respectively. These findings indicate that the POTI domains in the diblock copolymer thin film undergo a mesophase transition from a smectic-A to an isotropic phase near 245 °C during the heating run.

Figure 6d shows the 2D GISAXS pattern of a diblock copolymer film recorded at 245 °C. As can be seen in the figure, the GISAXS pattern at 245 °C contains several strong specular reflections along the $2\theta_f$ and α_f directions, which is quite different from the pattern obtained below 245 °C. In particular, three scattering features, marked P_1, P_2, and P_3 (see the GISAXS pattern in Figure 6d), appear along the $2\theta_f$ direction with relative scattering lengths from the specular reflection position of 1, $\sqrt{3}$, and $\sqrt{4}$. Furthermore, some oscillations are observed along the α_f direction at position P_1. These reflections in the GISAXS pattern are representative of a hexagonal structure of cylinders oriented perpendicular to the film plane.[11]

To examine this pattern in detail, the in-plane and out-of-scattering profiles in the GISAXS pattern measured at 245 °C in Figure 6d were extracted, as shown in Figures 6e and 6f, respectively. The in-plane scattering profiles were extracted at $\alpha_f = 0.18°$, and the out-of-plane scattering profiles were extracted at $2\theta_f = 0.31°$, where the first diffraction spot appeared. As can be seen in Figure 6e, the in-plane scattering profile at 245 °C contains three diffraction peaks with relative scattering vector lengths from the specular reflection position of 1, $\sqrt{3}$, and $\sqrt{4}$; the second spots are much weaker in intensity than the other spots. These scattering peaks are characteristic of a hexagonally packed cylinder structure, indicating that the cylindrical microdomains of the POTI blocks are aligned along a direction perpendicular to the film plane and are furthermore packed hexagonally in the film plane. The first order scattering peak at $2\theta_f = 0.31°$ corresponds to a *d*-spacing of 26.6 nm, and is assigned to the interdistance between the POTI cylinders oriented normal to the film plane in the PS matrix. In contrast to the in-plane scattering profile, the out-of-plane scattering profile at 245 °C in Figure 6f mainly consists of oscillations. These profiles resemble the specular X-ray reflectivity profiles of thin films, which are modulated by Kiessig fringes.[13] These fringes generally appear because of interference between the X-ray beams reflected from the film surface and those reflected from the film/substrate interface, namely the standing waves of the X-ray beam within the thin film. The film thickness can be estimated from the periodicity of the Kiessig fringes. The amplitude of the Kiessig fringes is often modulated at a lower frequency if there is a layer structure within the film. Furthermore, the out-of-plane scattering profiles show that no features characteristic of hexagonally packed POTI microdomains lie on the out-of plane axis, whereas such features are observed in the in-plane scattering profiles. These results indicate that the POTI microdomains formed in the film are preferentially oriented normal to the film plane and occupy the whole film thickness. In other words, the phase-separated POTI microdomains are formed in the films with cylindrical shapes and heights comparable to the film thickness, and are oriented in the out-of-plane direction.

To quantitatively analyze these profiles, we sought to fit the profiles measured at 245 °C using a previously derived GIXS formula with a hexagonal structure factor and a cylinder form factor.[11] As can be seen from the solid fit lines in Figure 6e,

Table 1. Structural Parameters of the PS-*b*-POTI Thin Film at 245 °C, Which Were Obtained by GISAXS Measurement and Data Analysis

d_{sp}[a] (nm)	$\bar{R}$[b] (nm)	σ_R[c] (nm)	h[d] (nm)	g[e]
26.6	5.7	1.95	23.5	0.075

[a] Center-to-center distance of cylinder (*d*-spacing of the hexagon). [b] Average cylinder radius determined from the peak maximum of the radius r and Gaussian distribution. [c] Standard deviation of cylinder radius. [d] Height of the cylinder. [e] Paracrystal distortion factor defined by $g = \Delta a/a$, where a and Δa are the fundamental vector of hexagon axis and its displacement, respectively.

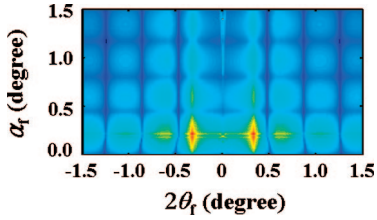

Figure 7. 2D GISAXS pattern simulated for the diblock copolymer film at 245 °C using the GISAXS formula with the structural parameters (listed in Table 1) obtained by analyzing the scattering data in Figure 6d.

the calculated scattering profile is in good agreement with the measured profiles, confirming that the measured GISAXS patterns were successfully analyzed. From this quantitative analysis, we obtained the important structural parameters at 245 °C: cylinder shape, radius and radius distribution, center-to-center distance, and degree of packing order; these parameters are summarized in Table 1.

Furthermore, by using these structural parameters, we sought to reconstruct the 2D GISAXS pattern using the GISAXS formula for a hexagonal paracrystal lattice of cylinders.[11] The reconstructed scattering pattern is presented in Figure 7. As can be seen in the figure, the calculated 2D GISAXS pattern is in good agreement with the scattering pattern measured at 245 °C in Figure 6d, confirming that the measured GISAXS pattern was successfully analyzed.

The GISAXS analysis therefore confirms that in the diblock copolymer film, the lamellar structure of the PS and POTI stacks is converted to a hexagonal cylinder structure when the POTI domains undergo the smectic-A to isotropic phase transition at 238 °C (Figure 3). This order-order transition of the PS-*b*-POTI block copolymer might be made possible by the enhancement of the mobility of the POTI domains that accompanies the smectic-A to isotropic phase transition. It was previously reported that some homopolymers,[14] diblock copolymers[15] and triblock copolymers[16] show a temperature-dependent order-order transition from a lamellar to a hexagonal cylinder structure. However, to the best of our knowledge, the present work constitutes the first report of an order-order transition of block copolymer thin films from lamellae to hexagonal cylinders with a preferred orientation.

To confirm the order-order transition of the PS-*b*-POTI thin film, we investigated the surface structure of the diblock copolymer film using an atomic force microscope. As can be seen in Figure 8a, the AFM surface image obtained at 25 °C shows a smooth and featureless surface structure. Thus, even though the GISAXS pattern for the PS-*b*-POTI thin film at 25 °C indicates a lamellar structure, no surface structure is evident in the AFM image. To observe the high-temperature surface structure of the PS-*b*-POTI thin film, the film was annealed at 245 °C for 1 h under vacuum and then quenched to room temperature. As can be seen in Figure 8b, the AFM surface image clearly shows the hexagonal packing of the cylindrical POTI domains oriented normal to the film plane. From the

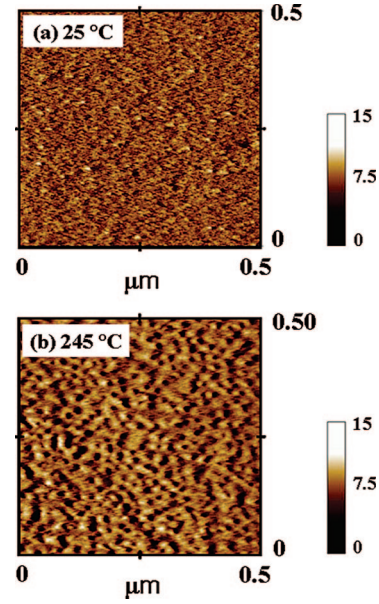

Figure 8. AFM phase images (500 nm × 500 nm) of the PS-*b*-POTI thin film deposited on a silicon substrate at (a) 25 °C or (b) the film annealed at 245 °C for 1 h under vacuum and quenched to room temperature.

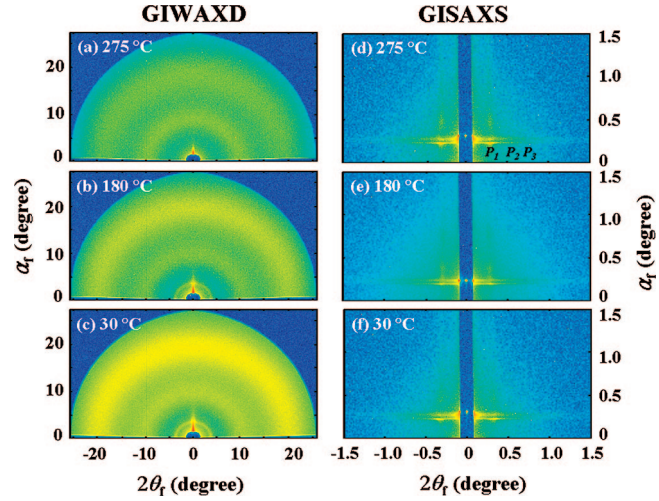

Figure 9. 2D GIWAXD and GISAXS patterns obtained at $\alpha_i = 0.18°$ for the PS-*b*-POTI thin film on a silicon substrate during cooling.

Fourier transform of the AFM phase image in Figure 8b, the interdistance between the cylindrical POTI domains was estimated to be 29.5 nm. This interdistance value is slightly larger than the value of 26.6 nm obtained from the analysis of the GISAXS data at 245 °C. These AFM images indicate that the PS-*b*-POTI block copolymer film undergoes an order-order transition to a hexagonal cylinder structure at 245 °C.

At the higher temperature of 285 °C, the GISAXS pattern was found to be featureless, while the GIWAXD pattern showed only amorphous halo peaks similar to those observed at 245 °C (data not shown). Similar featureless patterns were observed at temperatures up to 300 °C. These results indicate that no distinctive phase-separated structure is present in the film and that the diblock copolymer molecules in the film undergo an order−disorder transition near 285 °C.

Figure 9 shows the GIWAXD and GISAXS patterns obtained during cooling from 300 °C. As can be seen in Figure 9a, a featureless GIWAXD pattern except for two isotropic amorphous rings was observed. Below 190 °C, the transition temperature from an isotropic liquid to a smectic-A phase, the

GIWAXD pattern contains structural features. As can be seen in Figure 9b, the reflection peak due to the smectic-A phase appears at $\alpha_f = 3.61°$ (d-spacing = 2.44 nm). The GISAXS pattern at 180 °C during the cooling run closely resembles that obtained at the same temperature during the heating run, except for the weaker intensity of the former pattern. A similar GIWAXD pattern was obtained during further cooling to near 30 °C. However, as can be seen in Figure 9c, the intensity of the reflection peak at $\alpha_f = 3.63°$ (d-spacing = 2.43 nm) increased during the cooling run, indicating that the layer stacking order in the POTI domains was enhanced during cooling. It might be expected that the smectic A structure of POTI blocks would be enhanced by an appropriate annealing process. The d-spacing value of the reflection peak at $\alpha_f = 3.63°$ is the same as that of the reflection peak observed at 25 °C during the heating run, which corresponds to the layer spacing of the POTI blocks.

Parts d−f of Figure 9 show representative GISAXS patterns obtained during the cooling run from 300 °C. Featureless GISAXS patterns were observed during cooling to 280 °C. Below 280 °C, however, structural features are present in the GISAXS patterns. The GISAXS pattern at 275 °C (Figure 9d) closely resembles that obtained at the same temperature during the heating run, except for the weaker intensity of the former pattern. In particular, the scattering spot P_1 is clear, and P_2 and P_3 appear with weak intensities. We also found an oscillation pattern along the α_f direction at the P_1 position. This scattering pattern is characteristic of hexagonally packed cylinders oriented normal to the film plane, resulting from a disorder−order transition of the PS-*b*-POTI thin film.

Below 190 °C, the transition temperature from an isotropic liquid to a smectic-A phase, the GISAXS pattern observed at 180 °C during the cooling run still contains very weak peaks characteristic of hexagonally packed cylinders. In particular, the scattering spot P_1 and oscillation pattern along the α_f direction appeared with weak intensity, but P_2 and P_3 were not discernible. Taking into account the above GIWAXD pattern measured at the same temperature, this GISAXS pattern suggests that the order-order transition from a hexagonal cylinder structure to a lamellar structure is incomplete just below 190 °C.

As can be seen in Figure 9f, the scattering pattern obtained at 30 °C during the cooling run contains reflection spots with enhanced intensity along the $2\theta_f$ direction. We also found that the oscillation pattern along the α_f direction had nearly disappeared. These changes in the scattering patterns are attributed to the enhancement of the order-order transition from a hexagonal cylinder structure to a lamellar structure.

The above *in situ* GIWAXD and GISAXS results show that thin films of the PS-*b*-POTI diblock copolymer undergo interesting and complicated phase transitions as the temperature is varied. The phase transition processes observed during the cooling run were found to be reversible during the heating run. In particular, during the heating run a lamellar structure of PS and POTI domains was found to be converted to a hexagonal cylinder structure. The series of phase transformations in the film are depicted schematically in Figure 10.

Conclusions

In this study, synchrotron GIWAXD and GISAXS analyses were performed together with DSC measurements on semirod−coil PS-*b*-POTI diblock copolymer thin films supported on silicon substrates during heating to 300 °C and subsequent cooling to 30 °C. These analyses provided significant information about the morphologies of the phase-separated PS and POTI domains and the molecular structures formed in each domain. Thin films of the PS-*b*-POTI diblock copolymer undergo both temperature-dependent order−order and order-disorder phase transitions.

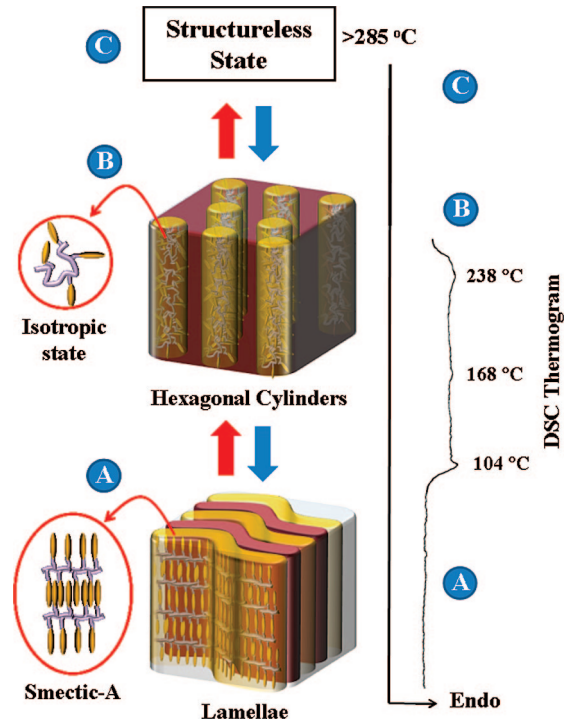

Figure 10. Proposed structural models of the phase transitions of the PS-*b*-POTI thin film during heating and cooling.

This study found that the diblock copolymer molecules in the thin film at 25 °C form an alternately stacked structure of amorphous PS and smectic-A POTI microdomains whose stacking direction is parallel to the film plane. During the heating run, the diblock copolymer undergoes phase separation near 245 °C and then forms a hexagonal cylinder structure oriented normal to the film plane with cylindrical POTI domains in the PS matrix, at which point the POTI domains and the PS matrix are both in amorphous liquid states. This conversion is induced by the transformation of the POTI domains from the smectic-A phase to the isotropic phase, where the smectic-A phase is composed of a laterally ordered structure of interdigitated bristles in the POTI blocks. The hexagonal cylinder structure that forms during heating is stable up to 280 °C. These temperature-dependent order-order and order−disorder phase transitions in the film are reversed during the cooling run. On the basis of the observed *in situ* GISAXS and GIWAXD results, temperature-dependent molecular structure models were established for the PS-*b*-POTI block polymer in thin films.

Acknowledgment. This study was supported by the Korea Science & Engineering Foundation (National Research Laboratory Program, and Center for Integrated Molecular Systems) and by the Ministry of Education, Science and Technology (MEST) (BK21 Program). Synchrotron GIXS measurements at the Pohang Accelerator Laboratory were supported by the MEST and the POSCO.

References and Notes

(1) (a) Bates, F. S.; Fredrickson, G. H. *Annu. Rev. Phys. Chem.* **1990**, *41*, 525. (b) Mansky, P.; Chaikin, P.; Thomas, E. L. *J. Mater. Sci.* **1995**, *30*, 1987. (c) Spatz, J. P.; Roescher, A.; Sheiko, S.; Krausch, G.; Moeller, M. *Adv. Mater.* **1995**, *7*, 731. (d) Ge, S.; Takahara, A.; Kajiyama, T. *Langmuir* **1995**, *11*, 1341. (e) Chou, S. Y.; Krauss, P. R.; Renstrom, P. J. *J. Vac. Sci. Technol. B* **1996**, *14*, 4129. (f) Park, M.; Harrison, C.; Chaikin, P. M.; Register, R. A.; Adamson, D. H. *Science* **1997**, *276*, 1401. (g) Herrninghaus, S.; Jacobs, K.; Mecke, K.; Bischof, J.; Fery, A.; Ibn-Elhaj, M.; Schlagowski, S. *Science* **1998**, *282*, 916. (h) Ryu, C. Y.; Lodge, T. P. *Macromolecules* **1999**, *32*, 7190. (i) Thurn-Albrecht, T.; Steiner, R.; DeRouchey, J.; Stafford, C. M.; Huang, E.; Ball, M.; Tuominen, M.; Hawker, C. J.; Russell, T. P. *Adv. Mater.*

2000, *12*, 787. (j) Shin, Y. C.; Choi, K.-Y.; Jin, M. Y.; Hong, S.-K.; Cho, D.; Chang, T.; Ree, M. *Kor. Polym. J.* **2001**, *9*, 100. (k) Kim, J.-S.; Kim, H.-C.; Lee, B.; Ree, M. *Polymer* **2005**, *46*, 7394. (l) Kim, J.-S.; Kim, H.; Yoon, J.; Heo, K.; Ree, M. *J. Polym. Sci.: Part A: Polym. Chem. Ed.* **2005**, *43*, 4079. (m) Ree, M.; Yoon, J.; Heo, K. *J. Mater. Chem.* **2006**, *16*, 685.

(2) (a) Park, C.; Rhue, M.; Im, M.; Kim, C. *Macromol. Res.* **2007**, *15*, 688. (b) Park, H.-W.; Im, K.; Chung, B.; Ree, M.; Chang, T. *Macromolecules* **2007**, *40*, 2603. (c) Park, S.; Ryu, D. Y.; Kim, J. K.; Ree, M.; Chang, T. *Polymer* **2008**, *49*, 2170. (d) Chung, B.; Choi, H.; Park, H.-W.; Ree, M.; Jung, J. C.; Zin, W. C.; Chang, T. *Macromolecules* **2008**, *41*, 1760. (e) Yang, S. Y.; Park, J.; Yoon, J.; Ree, M.; Jang, S. K.; Kim, J. K. *Adv. Funct. Mater.* **2008**, *18*, 1371. (f) Yoon, J.; Jung, S. Y.; Ahn, B.; Heo, K.; Jin, S.; Iyoda, T.; Yoshida, H.; Ree, M. *J. Phys. Chem. B.* **2008**, *112*, 8486.

(3) (a) Widawski, G.; Rawiso, M.; Francüois, B. *Nature* **1994**, *369*, 387. (b) Jenekhe, S. A.; Zhang, X.; Chen, X. L.; Choong, V.-E.; Gao, Y.; Hsieh, B. R. *Chem. Mater.* **1997**, *9*, 409. (c) Smith, R. C.; Fisher, W. M.; Gin, D. L. *J. Am. Chem. Soc.* **1997**, *119*, 4092. (d) Ng, S.-C.; Chan, H. S. O.; Xia, J.-F.; Yu, W. *J. Mater. Chem.* **1998**, *8*, 2347. (e) Marsitzky, D.; Klapper, M.; Mullen, K. *Macromolecules* **1999**, *32*, 8685. (f) Lee, M.; Cho, B.-K.; Zin, W.-C. *Chem. Rev.* **2001**, *101*, 3869. (g) Liu, J.; Sheina, E.; Kowalewski, T.; McCullough, R. D. *Angew.Chem., Int. Ed.* **2002**, *41*, 329. (h) Carswell, A. D. W.; O′Rear, E. A.; Grady, B. P. *J. Am. Chem. Soc.* **2003**, *125*, 14793. (i) Hatano, T.; Bae, A.-H.; Takeuchi, M.; Fujita, N.; Kaneko, K.; Ihara, H.; Takafuji, M.; Shinkai, S. *Angew. Chem., Int. Ed.* **2004**, *43*, 465.

(4) (a) Francüois, B.; Pitois, O.; FrancoisJ, *Adv. Mater.* **1995**, *7*, 1041. (b) Francüois, B.; Pitois, O.; Francois, J. *Adv. Mater.* **1995**, *7*, 1041. (c) de Boer, B.; Stalmach, U.; van.Hutten, P. F.; Melzer, C.; Krasnikov, V. V.; Hadziioannou, G. *Polymer* **2001**, *42*, 9097. (d) Vriezema, D. M.; Hoogboom, J.; Velonia, K.; Takazawa, K.; Christianen, P. C. M.; Maan, J. C.; Rowan, A. E.; Nolte, R. J. M. *Angew. Chem., Int. Ed.* **2003**, *42*, 772. (e) Cluendias, A.; Hellaye, M. L.; Lecommandoux, S.; Cloutet, E.; Cramail, H. *J. Mater. Chem.* **2005**, *15*, 3264. (f) Lee, K.-W.; Lin, H.-C. *Polymer* **2007**, *48*, 3664.

(5) Hayakawa, T.; Horiuchi, S. *Angew. Chem., Int. Ed.* **2003**, *42*, 2285.

(6) (a) Bolze, J.; Kim, J.; Huang, J.-Y.; Rah, S.; Youn, H. S.; Lee, B.; Shin, T. J.; Ree, M. *Macromol. Res.* **2002**, *10*, 2. (b) Lee, B.; Oh, W.; Yoon, J.; Hwang, Y.; Kim, J.; Landes, B. G.; Quintana, J. P.; Ree, M. *Macromolecules* **2005**, *38*, 8991. (c) Heo, K.; Jin, K. S.; Yoon, J.; Jin, S.; Oh, W.; Ree, M. *J. Phys. Chem. B* **2006**, *110*, 15887. (d) Choi, J. M.; Kang, S. Y.; Bae, W. J.; Jin, K. S.; Ree, M.; Cho, Y. *J. Biol. Chem.* **2007**, *282*, 9941. (e) Kim, D. Y.; Jin, K. S.; Kwon, E.; Ree, M.; Kim, K. K. *Proc. Natl. Acad. Sci. U.S.A.* **2007**, *104*, 8779. (f) Heo, K.; Park, S.-G.; Yoon, J.; Jin, K. S.; Jin, S.; Rhee, S.-W.; Ree, M. *J. Phys. Chem. C* **2007**, *111*, 10848. (g) Jin, K. S.; Kim, D. Y.; Rho, Y.; Le, V. B.; Kwon, E.; Kim, K. K.; Ree, M. *J. Synchrotron Rad.* **2008**, *15*, 219. (h) Lee, J. H.; Kang, G. B.; Lim, H.-H.; Jin, K. S.; Kim, S.-H.; Ree, M.; Park, C.-S.; Kim, S.-J.; Eom, S. H. *J. Mol. Biol.* **2008**, *376*, 308. (i) Jin, K. S.; Park, J. K.; Yoon, J.; Rho, Y.; Kim, J.-H.; Kim, E. E.; Ree, M. *J. Phys. Chem. B.* **2008**, *112*, 9603. (j) Yoon, J.; Kim, K.-W.; Kim, J.; Heo, K.; Jin, K. S.; Jin, S.; Shin, T. J.; Lee, B.; Rho, Y.; Ahn, B.; Ree, M. *Macromol. Res.* **2008**, *16*, 625. (k) Yang, C.; Yoon, J.; Kim, S. H.; Hong, K.; Heo, K.; Ree, M.; Park, C. E. *Appl. Phys. Lett.* **2008**, *92*, 243305.

(7) Ree, M.; Ko, I. S. *Phys. High Tech.* **2005**, *14*, 2.

(8) (a) Rauscher, M.; Salditt, T.; Spohn, H. *Phys. Rev. B.* **1995**, *52*, 16855. (b) Sinha, S. K.; Sirota, E. B.; Garoff, S.; Stanley, H. B. *Phys. Rev. B* **1988**, *38*, 2297. (c) Holy, V., Pietsch, U.; Baumbach, T. *High-resolution X-ray scattering from thin films and multilayers*; Springer-Verlag: Berlin, 1999. (d) Tolan, M. *X-ray scattering from soft matter thin films*; Springer-Verlag: Berlin, 1999. (e) Lee, B.; Park, Y.-H.; Hwang, Y.-T.; Oh, W.; Yoon, J.; Ree, M. *Nat. Mater.* **2005**, *4*, 147. (f) Lee, B.; Oh, W.; Hwang, Y.; Park, Y. H.; Yoon, J.; Jin, K. S.; Heo, K.; Kim, J.; Kim, K.-W.; Ree, M. *Adv. Mater.* **2005**, *17*, 696.

(9) (a) Lee, B.; Park, I.; Yoon, J.; Park, S.; Kim, J.; Kim, K.-W.; Chang, T.; Ree, M. *Macromolecules* **2005**, *38*, 4311. (b) Lee, B.; Yoon, J.; Oh, W.; Hwang, Y.-T.; Heo, K.; Jin, K. S.; Kim, J.; Kim, K.-W.; Ree, M. *Macromolecules* **2005**, *38*, 3395. (c) Park, I.; Lee, B.; Ryu, J.; Im, K.; Yoon, J.; Ree, M.; Chang, T. *Macromolecules* **2005**, *38*, 10532. (d) Busch, P.; Rauscher, M.; Smilgies, D.-M.; Posselt, D.; Papadakis, C. M. *J. Appl. Crystallogr.* **2006**, *39*, 433. (e) Jin, S.; Yoon, J.; Heo, K.; Park, H.-W.; Shin, T.; Chang, T.; Ree, M. *J. Appl. Crystallogr.* **2007**, *40*, 950. (f) Heo, K.; Yoon, J.; Jin, S.; Kim, J.; Kim, K.-W.; Shin, T. J.; Chung, B.; Chang, T.; Ree, M. *J. Appl. Crystallogr.* **2008**, *41*, 281.

(10) (a) Yoon, J.; Choi, S.; Jin, S.; Jin, K. S.; Heo, K.; Ree, M. *J. Appl. Crystallogr.* **2007**, *40*, s669. (b) Yoon, J.; Jin, K. S.; Kim, H. C.; Kim, G.; Heo, K.; Jin, S.; Kim, J.; Kim, K.-W. *J. Appl. Crystallogr.* **2007**, *40*, 476. (c) Kim, G.; Yoon, J.; Kim, J.-S.; Kim, H.; Ree, M. *J. Phys. Chem. B.* **2008**, *112*, 8868.

(11) Yoon, J.; Yang, S. Y.; Lee, B.; Joo, W. C.; Kim, J. K.; Ree, M. *J. Appl. Crystallogr.* **2007**, *40*, 305.

(12) (a) Fichou, D., Ed. *Handbook of Oligo- and Polythiophenes*; Wiley-VCH: Weinheim, Germany, 1999. (b) Scherlis, D. A.; Marzari, N. *J. Am. Chem. Soc.* **2005**, *127*, 3207.

(13) Bolze, J.; Ree, M.; Youn, H. S.; Chu, S.-H.; Char, K. *Langmuir* **2001**, *17*, 6683.

(14) Yoon, J.; Lee, S. W.; Choi, S.; Heo, K.; Jin, S.; Kim, G.; Kim, H.; Ree, M. *J. Phys. Chem. B* **2008**, *112*, 5338.

(15) (a) Hamley, I. W.; Koppi, K. A.; Rosedale, J. H.; Bates, F. S.; Almdal, K.; Mortensen, K. *Macromolecules* **1993**, *26*, 5959. (b) Ruokolainen, J.; Makinen, R.; Torkkeli, M.; Makela, T.; Serimaa, R.; ten Brinke, G.; Ikkala, O. *Science* **1998**, *280*, 557.

(16) Jeong, U.; Aida, S.; Lee, H. H.; Kim, J. K.; Okamoto, S.; Sakurai, S. *Macromolecules* **2003**, *36*, 1685.

MA801727R